

Equation (4.8) reduces to an identity both in exact $SU(3)$ and in exact $SU(6)_W$; this relation has also been derived in broken $SU(3)$.¹³ It is known that Eq. (4.8) is very well satisfied experimentally.¹³

(vi) Another relation which follows in the broken and exact $SU(6)_W$ is the following:

$$\langle \pi^- p | \pi^- N^{*+} \rangle = (1/2\sqrt{3}) \langle \pi^- p | \pi^+ N^{*-} \rangle. \quad (4.9)$$

Such a simple type of relation does not exist in $SU(3)$. It has been shown by Olsson¹⁴ that a relation of the type (4.9) is very well satisfied experimentally.

V. CONCLUSION

In conclusion, we wish to emphasize that the broken $SU(6)_W$ successfully eliminates many of the bad predictions of exact $SU(6)_W$ and of exact $SU(6)_S$ and retains some of the good results as far as baryon-meson scattering is concerned. Similarly when one of the final scattered particles is a baryon resonance, some of the bad features disappear; at the same time some of the

¹³ S. Meshkov, G. A. Snow, and G. B. Yodh, Phys. Rev. Letters **13**, 212 (1964).

¹⁴ M. G. Olsson, Phys. Rev. Letters **15**, 710 (1965).

good results retain their validity. It is important to notice that the symmetry-breaking interaction which we have used to break the $SU(6)_W$ symmetry is isospin conserving and can not alter the exact $SU(6)_W$ ratio between two isospin amplitudes for processes in which the members of the same isomultiplets are involved. Thus the nonvalidity of the Johnson-Treiman relations involving reactions with different isospin multiplets is easily understood. The validity or nonvalidity of all other relations like the ones discussed in Secs. III and IV can similarly be explained.

ACKNOWLEDGMENTS

The author would like to express his deep gratitude to Dr. Gyan Mohan for his guidance throughout the course of this investigation. He is extremely grateful to Professor R. C. Majumdar for his constant encouragement and for the facilities provided in the Physics Department. He wishes to express his sincere gratitude to Professor S. N. Biswas for several helpful discussions. Finally he would like to thank Dr. L. K. Pande for his generous collaboration in the early stages of this calculation and for pointing out an error in the manuscript.

Observable Effects of the Leading Landau Singularity of the Box Graph*

PETER COLLAS AND RICHARD E. NORTON

Department of Physics, University of California, Los Angeles, California

(Received 19 December 1966; revised manuscript received 20 March 1967)

The effect of the leading Landau singularity of the fourth-order single-loop graph in a two-particle to four-particle amplitude is investigated. The amplitude for the graph is evaluated from a dispersion relation in the mass squared of the two particles interacting in the final state, and its behavior is studied using a simple model. The reactions $\bar{p}p \rightarrow \bar{K}K\pi\pi$ and $\bar{p}p \rightarrow \Lambda\Lambda\pi^+\pi^-$ are examined in some detail, and peaks are predicted for the amplitude squared in a certain range of the external variables.

I. INTRODUCTION

IT is of some interest to investigate the possibility that the singularities associated with some graphs may under certain circumstances have *direct* physical manifestations.

The possibility of an experimentally observable effect arising from triangle graphs has been the subject of intense investigation.¹ Unfortunately, the leading

Landau singularity of the triangle graph is a logarithmic branch point and is thus rather "weak"; attempts to reinforce the amplitude enhancement by combining this logarithmic singularity with the inverse square root non-Landau branch point of the triangle (see, for example, Landshoff, Treiman, Halpern, and Watson¹) have met with limited success (see, for example, Month, but also Cason *et al.*, in Ref. 1). This is due to the fact that the non-Landau branch point is always on an unphysical Riemann sheet and only under special circumstances can it approach the normal threshold; one has in fact to impose stringent mass constraints at

* Partially supported by the National Science Foundation. Based, in part, on a thesis submitted by P. Collas to the University of California at Los Angeles in partial fulfillment of the requirements for the degree of Doctor of Philosophy.

¹ P. V. Landshoff and S. B. Treiman, Phys. Rev. **127**, 649 (1962); R. Aaron, Phys. Rev. Letters **10**, 32 (1963); F. R. Halpern and H. L. Watson, Phys. Rev. **131**, 2674 (1963); I. J. R. Aitchison, *ibid.* **133**, B1257 (1964); V. V. Anisovich and L. G. Dakhno, Phys. Letters **10**, 221 (1964); C. Goebel, *ibid.* **13**, 143 (1964); C. Kascser, *ibid.* **12**, 269 (1964); Y. F. Chang and S. F. Tuan, Phys. Rev.

136, B741 (1964); M. Month, Phys. Letters **18**, 357 (1965). Phys. Rev. **139**, B1093 (1965); *ibid.* **151**, 1302 (1966); N. M. Cason, S. Mikamo, and A. Subramanian, Phys. Rev. Letters **17**, 838 (1966); C. Schmid, Phys. Rev. **154**, 1363 (1967); J. B. Bronzan, *ibid.* **134**, B687 (1964).

each vertex, which force the whole graph to "take place" at threshold. These constraints are not easily satisfied in practice, and as a result on the one hand it is very difficult to find cases suitable for investigation, and on the other any visible effect is extremely sensitive to the variation of the incoming energy, etc. Our purpose here is to examine in some detail the variation of the amplitude for the so-called box graph (Fig. 1). The leading Landau singularity of this graph is an inverse square root branch point, and therefore it is reasonable to expect that under the proper conditions (*viz.*, when the singularity is close to the physical boundary) it may give rise to a relatively strong peaking effect as compared with the (logarithmic) triangle case. As we shall see, the box singularity can in general be made to appear *anywhere* along the physical boundary and does not require any stringent vertex constraints. Moreover, one can find processes for which a strong effect persists for small ranges of the external variables and for which the vertices can be justifiably expected to be large.

In Sec. II we study the Landau curves of the singularities involved. For our purpose the box amplitude is most conveniently represented by a dispersion relation in the mass squared of the two particles interacting in the final state. This also is derived in Sec. II for a general process of the type $A+B \rightarrow C+D+E+F$. In Sec. III we introduce widths for the unstable particles (resonances)² in the intermediate state and study, using a model process, the motion of the singularities and the subsequent behavior of the amplitude as a function of the external variables and widths. Finally in Sec. IV we consider the reactions $\bar{p}p \rightarrow \bar{K}K\pi\pi$ and $\bar{p}p \rightarrow \bar{\Lambda}\Lambda\pi^+\pi^-$ and investigate the possibility of amplitude enhancements arising from the graphs of Fig. 17.

Readers interested only in our experimental predictions can skip Sec. II and Sec. III and go directly to Sec. IV.

II. DERIVATION OF THE DISPERSION RELATION

A. Preliminaries

There are essentially three different configurations for processes proceeding via the box graph³ (see Fig. 1); any other can be obtained from one of these by re-labeling the vertices.

We restrict ourselves to the case of only two incoming particles. Wiggly lines represent unstable particles.

Process (c) of Fig. 1 is experimentally unfeasible, since it requires two unstable particles in the initial state. For definiteness, and also because the mechanism of Fig. 1(a) requires the relatively rare occurrence of a

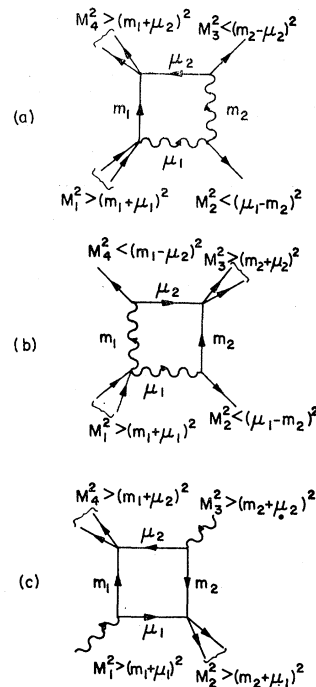


FIG. 1. The three possible configurations of the box graph.

resonance decaying into another resonance, we have restricted ourselves to a study of the configuration shown in Fig. 1(b). Although the process of Fig. 1(a) may contribute to significant mass peakings, it is expected that this would occur when the external momenta are outside the range for which the mechanism of Fig. 1(b) is important. Hence, it is reasonable that the two possible sources of mass peakings shown in Fig. 1(a) and 1(b) be studied separately.

We would expect a large contribution to the amplitude from the box graph [Fig. 1(b)] when the corresponding box singularity is "close" to the physical boundary⁴ for the process of interest provided the amplitudes occurring at the vertices of our graph are "large."⁵

We denote the external 4-momenta by p_i ; thus $p_i^2 = -M_i^2$. We also define the two invariant variables s, t :

$$\begin{aligned} s &= -(p_1 - p_2)^2 = -(p_3 + p_4)^2, \\ t &= -(p_1 - p_4)^2 = -(p_2 + p_3)^2. \end{aligned} \quad (1)$$

The invariant amplitude for the box graph depends on the six invariants: $M_1^2, M_2^2, M_3^2, M_4^2, s, t$. Our mathematical expressions take a simpler form if we use instead the following six dimensionless variables⁶

⁴ The *physical boundary* of a complex amplitude is the set of points of the *physical sheet* which lies in the *physical range* of the external variables of the amplitude.

⁵ A more precise meaning of these statements will be given later on.

⁶ R. Karplus, C. M. Sommerfield, and E. H. Wichmann, Phys. Rev. 114, 376 (1959).

² For a justification of this procedure see I. J. R. Aitchison and C. Kacser, Phys. Rev. 133, B1239 (1964).

³ R. E. Norton, Phys. Rev. 135, B1381 (1964); S. Coleman and R. E. Norton, Nuovo Cimento 38, 438 (1965); R. J. Eden, Phys. Rev. 119, 1763 (1960).

(see Fig. 1 for significance of symbols):

$$\begin{aligned} x &= \frac{s - m_1^2 - m_2^2}{2m_1 m_2}, & y &= \frac{t - \mu_1^2 - \mu_2^2}{2\mu_1 \mu_2}, \\ x_1 &= \frac{M_1^2 - \mu_1^2 - m_1^2}{2\mu_1 m_1}, & x_2 &= \frac{M_2^2 - \mu_1^2 - m_2^2}{2\mu_1 m_2}, \\ x_3 &= \frac{M_3^2 - \mu_2^2 - m_2^2}{2\mu_2 m_2}, & x_4 &= \frac{M_4^2 - \mu_2^2 - m_1^2}{2\mu_2 m_1}. \end{aligned} \quad (2)$$

In terms of these variables the inequalities ("instability" conditions) in Fig. 1(b) become $x_1 > 1$, $x_2 < -1$, $x_3 > 1$, $x_4 < -1$.

It is convenient to write a dispersion relation for the box amplitude B in the variable x_3 and to investigate the amplitude enhancement in the x_3 physical range. Clearly, since the definition of x_3 [Eq. (2)] does not involve the internal masses μ_1 and m_1 of the unstable particles, our integration contour will remain on the real x_3 axis even after continuation to complex masses.

We shall thus be concerned with the singularities of B on its x_3 Riemann surface. These are, apart from the normal threshold at $x_3 = +1$, the triangle singularities⁷

$$L_{y_2^\pm} = -yx_2 \pm [(y^2 - 1)(x_2^2 - 1)]^{1/2}, \quad (3a)$$

$$L_{x_4^\pm} = -xx_4 \pm [(x^2 - 1)(x_4^2 - 1)]^{1/2}, \quad (3b)$$

and the box singularities⁸

$$\begin{aligned} x_3^\pm &= \frac{1}{(x_1^2 - 1)} \{ x_1(yx + x_2x_4) + yx_2 + xx_4 \\ &\quad \pm [(x_1 - L_{y_4^-})(x_1 - L_{y_4^+}) \\ &\quad \times (x_1 - L_{x_2^-})(x_1 - L_{x_2^+})]^{1/2} \}. \end{aligned} \quad (4)$$

To orient ourselves we begin by reviewing briefly certain pertinent facts about the triangle and box singularities: viz., the conditions under which they appear on the physical boundary³ and their motion as some of the invariants are continued along certain paths.

As an example consider the process of Fig. 2(a) which is obtained by reducing the graph of Fig. 1(b). The triangle singularity $L_{y_2^-}$ of the graph lies on the physical boundary of the x_3 plane when

$$x_2 < -1, \quad y > +1, \quad y + x_2 < 0; \quad (5)$$

then $L_{y_2^-} > 1$. These conditions arise from requiring

⁷ On the x_1 Riemann surface we have the triangle singularities $L_{y_4^\pm}$ and $L_{x_2^\pm}$ defined analogously. We take all square roots to be positive for $x > 1$, $y > 1$, $x_2 < -1$, $x_4 < -1$.

⁸ On the x_1 Riemann surface we have the box singularities

$$\begin{aligned} x_1^\pm &= \frac{1}{(x_3^2 - 1)} \{ x_3(yx + x_2x_4) + yx_4 + xx_2 \\ &\quad \pm [(x_3 - L_{y_2^-})(x_3 - L_{y_2^+})(x_3 - L_{x_4^-})(x_3 - L_{x_4^+})]^{1/2} \}. \end{aligned}$$

We again take all square roots to be positive for x_1 , $x_3 > L_{x_i^\pm}$, $L_{y_j^\pm}$.

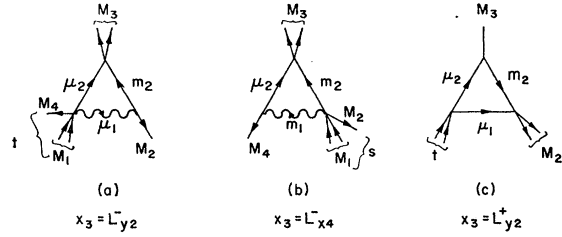


FIG. 2. By contracting the internal lines with masses m_1 and μ_1 in the graph of Fig. 1(b) one obtains the triangle graphs shown in (a) and (b), respectively. The triangle shown in (c) arises from contracting the line of mass m_1 in the diagram of Fig. 1(b) and reversing the direction of m_2 . For the three cases indicated, the triangle singularities $L_{y_2^-}$, $L_{x_4^-}$, and $L_{y_2^+}$ are singular on the physical boundary of the amplitude when the external momenta allow real internal particles to propagate in the directions given by the arrows.

positive Feynman parameters and real external momenta.³

The singularity $L_{y_2^+}$ on the other hand will lie on the physical boundary only when x_3 is a "momentum-transfer" variable, i.e., $x_3 < -1$; e.g. for the process shown in Fig. 2(c). So that when conditions (5) hold, it is on the wrong sheet.

In Fig. 3 we show the paths of $L_{y_2^\pm}$ as we continue $x_2 + i\epsilon$, ($\epsilon > 0$), from the region $x_2 < -1$, $y > 1$, $y + x_2 < 0$, to the region $x_2 < -1$, $y > 1$, $y + x_2 > 0$.

We now turn our attention to the box singularities [Eq. (4) and Ref. 8]. In Table I we give the conditions on the x_i , x , y , $L_{x_i^\pm}$, $L_{y_j^\pm}$ for the box singularity to lie on the physical boundary. These conditions follow from kinematical and geometrical requirements imposed so that the graph be realizable as a "classical process."⁸ When things are adjusted as in any of the four cases of Table I, the singularity $x_1^+(x_3)$ of the graph of Fig. 1(b) is on the physical boundary if, and only if, x_3 lies in the appropriate region indicated. When $x_1 = x_1^+(x_3)$ is on the physical boundary of the x_1 plane, $x_3 = x_3^+(x_1)$ is also on the physical boundary of the x_3 plane and vice versa. Inequalities such as $x + x_4 < 0$ imply that at least one L^- triangle singularity (e.g., $L_{x_4^-}$) will also be on the physical boundary. The singularities x_1^- and x_3^- appear on the physical boundary in processes for which x_1 and x_3 are "momentum-transfer" variables, i.e., $x_1, x_3 < -1$; therefore box singularities with opposite signature are never on the physical boundary at the same time.

In Fig. 4 we show the motion of the box singularities x_1^\pm , x_3^\pm as x_3 and x_1 , respectively, follow certain paths

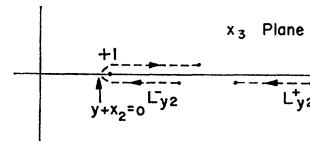


FIG. 3. Paths of $L_{y_2^\pm}$ as we go from $y + x_2 < 0$ to $y + x_2 > 0$ by increasing x_2 , keeping $x_2 < -1$ and $x > 1$ throughout the continuation. $L_{y_2^-}$ leaves the physical boundary by looping around the normal threshold at $x_3 = 1$. $L_{y_2^+}$ is never singular when $x_2 < -1$.

TABLE I. Conditions restricting box singularity to the physical boundary.
Restrictions on the x_i, x, y : $x_1, x_3, x, y > +1, x_2, x_4 < -1$.

Restrictions on the L_{xi^\pm}, L_{yi^\pm}	Location of box singularity in x_1 and x_3
$x+x_4 < 0, 1 < L_{y2}^- < L_{x4}^- < L_{y2}^+ < L_{x4}^+,$ then $1 < L_{x2}^- < L_{y4}^- < L_{x2}^+ < L_{y4}^+, y+x_4 < 0$	$L_{x4}^- < x_3 < x_3^0 < L_{y2}^+$ $x_3^0 \ni: x_1^+(x_3^0) = L_{y4}^-;$ then $L_{y4}^- < x_1 = x_1^+(x_3) < x_1^+(L_{x4}^-) < L_{x2}^+$
$1 < L_{y2}^- < L_{x4}^- < L_{x4}^+ < L_{y2}^+,$ then $1 < L_{y4}^- < L_{x2}^- < L_{x2}^+ < L_{y4}^+, x+x_2 < 0$	$L_{x4}^- < x_3 < x_3^0 < L_{x4}^+$ $x_3^0 \ni: x_1^+(x_3^0) = L_{x2}^-;$ then $L_{x2}^- < x_1 = x_1^+(x_3) < x_1^+(L_{x4}^-) < L_{x2}^+$
$y+x_2 < 0, 1 < L_{x4}^- < L_{y2}^- < L_{x4}^+ < L_{y2}^+,$ then $1 < L_{y4}^- < L_{x2}^- < L_{y4}^+ < L_{x2}^+, x+x_2 < 0$	$L_{y2}^- < x_3 < x_3^0 < L_{x4}^+$ $x_3^0 \ni: x_1^+(x_3^0) = L_{x2}^-;$ then $L_{x2}^- < x_1 = x_1^+(x_3) < x_1^+(L_{y2}^-) < L_{y4}^+$
$1 < L_{x4}^- < L_{y2}^- < L_{y2}^+ < L_{x4}^+,$ then $1 < L_{x2}^- < L_{y4}^- < L_{y4}^+ < L_{x2}^+, y+x_4 < 0$	$L_{y2}^- < x_3 < x_3^0 < L_{y2}^+$ $x_3^0 \ni: x_1^+(x_3^0) = L_{y4}^-$ then $L_{y4}^- < x_1 = x_1^+(x_3) < x_1^+(L_{y2}^-) < L_{y4}^+$

on their real axes, the remaining variables being restricted in the following domains (cf. Table I):

$$x > 1, \quad y > 1, \quad x_2 < -1, \quad x_4 < -1, \quad (6)$$

$$x+x_2 < 0, \quad x+x_4 < 0, \quad y+x_2 < 0, \quad y+x_4 < 0. \quad (7)$$

Thus a possible arrangement of the L^\pm is

$$+1 < L_{y2}^- < L_{x4}^- < L_{x4}^+ < L_{y2}^+ \quad \text{on the } x_3 \text{ plane,} \quad (8)$$

$$+1 < L_{y4}^- < L_{x2}^- < L_{x2}^+ < L_{y4}^+ \quad \text{on the } x_1 \text{ plane.} \quad (9)$$

Inequalities (6) and (7) imply that all L^- branch points are on the physical boundary.

If we let $x_2 = x_4$ and $x = y$ while preserving the inequalities (6) and (7), we have

$$\begin{aligned} x_2 = x_4 < -1, \\ x = y > +1, \\ \text{and} \quad x+x_2 < 0. \end{aligned} \quad (10)$$

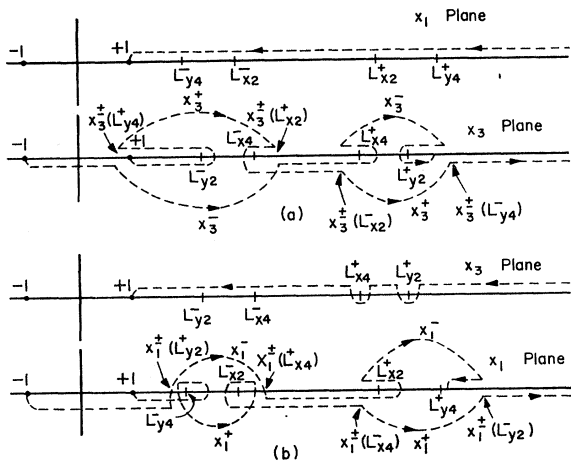


FIG. 4. Motion of the box singularities as functions of x_3 and x_1 . In the case shown [i.e., inequalities (6)-(9)], x_3^+ is on the physical boundary in (a) only on the segment of its trajectory on the real x_3 axis characterized by $dx_3^+(x_1)/dx_1 < 0$,

$$x_3^+ \in [L_{y2}^-, L_{y2}^+] \cap [L_{x4}^-, L_{x4}^+]; \text{ (cf. Table I).}$$

Then, from Eqs. (3) and (4),

$$\begin{aligned} L_{y2}^- = L_{x4}^- = L_{y4}^- = L_{x2}^-, \\ L_{y2}^+ = L_{x4}^+ = L_{y4}^+ = L_{x2}^+; \end{aligned} \quad (11)$$

and⁹

moreover,

$$x_3^+(x_1) = \frac{(x+x_2)^2}{x_1-1} + 1, \quad x_3^-(x_1) = \frac{(x-x_2)^2}{x_1+1} - 1, \quad (12)$$

and

$$x_1^+(x_3) = \frac{(x+x_2)^2}{x_3-1} + 1, \quad x_1^-(x_3) = \frac{(x-x_2)^2}{x_3+1} - 1. \quad (13)$$

Also, it is easy to show that as x_1 varies in $[+1, +\infty]$

$$x_3^+(x_1) \geq (<) x_3^-(x_1)$$

$$\text{when } (x_1 - L_{x2}^-)(x_1 - L_{x2}^+) \geq (<) 0, \quad (14)$$

while

$$x_3^+(L_{x2}^\pm) = x_3^-(L_{x2}^\pm) = L_{x2}^\mp,$$

and that analogous relations hold for the $x_1^\pm(x_3)$.

The rather complicated trajectories of $x_1^\pm(x_3)$ and $x_3^\pm(x_1)$ (Fig. 4) reduce now to the simple paths shown in Fig. 5. Finally we derive the limits of the physical range of x_3 or M_3^2 . From energy-momentum conserva-

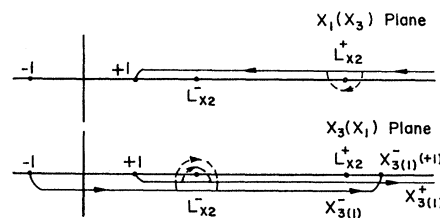


FIG. 5. Motion of the box singularities when $x_2 = x_4$ and $x = y$.

⁹ Under the circumstances we shall refer to the triangle singularities simply as L_{x2}^\pm .

tion we have, in the M_1 rest frame,

$$M_3^2 = (2M_1^2)^{-1} \{ -M_1^4 + M_1^2(s+t+M_2^2+M_4^2) - (s-M_2^2)(M_4^2-t) - \cos\phi \times [\Delta(s, M_1^2, M_2^2)\Delta(t, M_1^2, M_4^2)]^{1/2} \}, \quad (15)$$

where ϕ is the angle between \mathbf{p}_2 and \mathbf{p}_4 (recall that $p_i^2 = -M_i^2$), and $\Delta(a, b, c) = a^2 + b^2 + c^2 - 2ab - 2ac - 2bc$. Equation (15) for given $M_1^2, M_2^2, M_4^2, s, t$ limits the physical M_3^2 in the range

$$M_3^2(\cos\phi = +1) \leq M_3^2 \leq M_3^2(\cos\phi = -1). \quad (16)$$

Also, if ν_1 and ν_2 are the rest masses of the two particles which make up M_3^2 [see Fig. 1(b)], we have

$$M_3^2 \geq (\nu_1 + \nu_2)^2. \quad (17)$$

If we now let $M_2 = M_4 \equiv M, \nu_1 = \nu_2 = m_2 = \mu_2 \equiv \mu, m_1 = \mu_1 \equiv m$ [see Fig. 1(b)], and $s = t$, i.e., $x_2 = x_4, x = y$, the ranges (16) and (17) on the x_3 plane become¹⁰

$$\text{Max} \left\{ +1, \frac{2s + 2M^2 - M_1^2}{2\mu^2} - 1 \right\} \leq x_3 \leq x_3^-. \quad (18)$$

It is obvious that, in this simplified case, $x_3^+(x_1)$ can lie on the physical boundary *only* in the interval $[L_{x_2}^-, L_{x_2}^+]$, i.e. when $L_{x_2}^- \leq x_1 \leq L_{x_2}^+$, since only then $x_3^+ \leq x_3^-$ [see inequalities (14)].^{11,12}

B. The Dispersion Relation

In what follows we shall neglect particle spins and any structure at the vertices. This simplification is based on the hope that in the region of interest, viz., in the vicinity of the box singularity, the variation of the amplitude will be dominated by the box singularity, so that other effects will not be significant. (In this connection see the 1966 paper by Month in Ref. 1.) We shall return, however, to this subject in Sec. IV.

We proceed now to derive a dispersion relation in the x_3 variable for the situation determined by inequalities

¹⁰ It is also clear that since x_3^- now does not depend on m , it remains real when $m \rightarrow m - i\alpha$, while if $x \neq y, x_3^-(m - i\alpha)$ becomes complex and of course the upper end of the physical boundary is no longer x_3^- .

¹¹ We remark at this point that when $x_1 > L_{x_2}^+$, the upper limit of the x_3 physical range, viz., x_3^- , lies to the left of $L_{x_2}^+$, which implies that $L_{x_2}^-$ is no longer on the physical boundary, in spite of the fact that it still satisfies the conditions derived in Ref. 3 ($x + x_2 < 0$, etc.). These conditions, however, always involved the three external variables associated with the vertices of the triangle graph, and *no constraint was imposed on the other independent invariants*; it is precisely this kind of constraint that we introduced when we set $x = y$ (Ref. 12), and it is for this reason that now we need an extra condition for $L_{x_2}^-$ to be on the physical boundary, viz.:

$$1 + \frac{2m\mu(x+x_2) - \mu^2(L_{x_2}^- - 1)}{m^2} \leq x_1 \leq L_{x_2}^+.$$

When x_1 goes below the lower limit then

$$(2s + 2M^2 - M_1^2)/2\mu^2 - 1 > L_{x_2}^-.$$

¹² The important thing is that we fixed y , not that we fixed it equal to x .

(6), (7), (8), (9), and

$$L_{x_2}^- < x_1 < x_1^\pm(L_{x_4}^-). \quad (19)$$

Under the circumstances the branch points $+1, L_{y_2}^-, L_{x_4}^-,$ and x_3^+ are all on the physical boundary of the x_3 plane while $x_3^-, L_{x_4}^+,$ and $L_{y_2}^+$ are not. (Cf. Table I, second case from top, and Fig. 4.) Thus we can write¹³

$$B = \frac{1}{2\pi i} \int_1^\infty dx_3' \frac{\text{disc}_1 B[L_{y_2}^-(-), L_{x_4}^-(-), x_3^+(-)]}{x_3' - x_3} + \frac{1}{2\pi i} \int_{L_{y_2}^-}^\infty dx_3' \frac{\text{disc}_{L_{y_2}^-} B[L_{x_4}^-(-), x_3^+(-)]}{x_3' - x_3} + \frac{1}{2\pi i} \int_{L_{x_4}^-}^\infty dx_3' \frac{\text{disc}_{L_{x_4}^-} B[x_3^+(-)]}{x_3' - x_3} + \frac{1}{2\pi i} \int_{x_3^+}^\infty dx_3' \frac{\text{disc}_{x_3^+} B}{x_3' - x_3}. \quad (20)$$

Each contour runs above the corresponding cut and all of them pass *under* the branch points $x_3^-, L_{x_4}^+, L_{y_2}^+$; that this is the correct prescription will be shown later.

Now $\text{disc}_1 B$ has all the singularities of B , and it is clear that

$$\frac{1}{2\pi i} \int_1^\infty dx_3' \frac{\text{disc}_1 B[L_{y_2}^-(-), L_{x_4}^-(-), x_3^+(-)]}{x_3' - x_3} = \frac{1}{2\pi i} \int_1^\infty dx_3' \frac{\text{disc}_1 B[L_{y_2}^-(+), L_{x_4}^-(-), x_3^+(-)]}{x_3' - x_3} - \frac{1}{2\pi i} \int_{L_{y_2}^-}^\infty dx_3' \frac{\text{disc}_{L_{y_2}^-} \{ \text{disc}_1 B[L_{x_4}^-(-), x_3^+(-)] \}}{x_3' - x_3}. \quad (21)$$

Since the last integral on the right-hand side of Eq. (21) is equal to

$$\frac{1}{2\pi i} \int_{L_{y_2}^-}^\infty dx_3' \frac{\text{disc}_{L_{y_2}^-} B[L_{x_4}^-(-), x_3^+(-)]}{x_3' - x_3},$$

we have that

$$B = \frac{1}{2\pi i} \int_1^\infty dx_3' \frac{\text{disc}_1 B[L_{y_2}^-(+), L_{x_4}^-(-), x_3^+(-)]}{x_3' - x_3} + \frac{1}{2\pi i} \int_{L_{x_4}^-}^\infty dx_3' \frac{\text{disc}_{L_{x_4}^-} B[x_3^+(-)]}{x_3' - x_3} + \frac{1}{2\pi i} \int_{x_3^+}^\infty dx_3' \frac{\text{disc}_{x_3^+} B}{x_3' - x_3}.$$

¹³ By $\text{disc}_1 B[L_{y_2}^-(+), L_{x_4}^-(-), x_3^+(-)]$, for example, we mean the discontinuity of B across the normal threshold ($x_3 = +1$) continued *above* $L_{y_2}^-$ and *under* x_3^+ .

Continuing in the same way, we finally obtain

$$B = \frac{1}{2\pi i} \int_1^\infty dx'_3 \frac{\text{disc}_1 B(x'_3)}{x'_3 - x_3}, \quad (22)$$

where the contour goes *over* $L_{y_2^-}, L_{x_4^-}, x_3^+,$ and *under* $x_3^-, L_{x_4^+}, L_{y_2^+}.$

The discontinuity across the normal threshold cut on the x_3 plane, $\text{disc}_1 B,$ can be calculated by Cutkosky's rules.¹⁴ However, since the Feynman amplitude for the box graph is a symmetric function with respect to

$$f(x'_3) = \frac{1}{\pi\sqrt{K}} \ln \left[\frac{x_1^+(x'_3) + x_1^-(x'_3) - 2x_1 + 2\{[x_1^-(x'_3) - x_1][x_1^+(x'_3) - x_1]\}^{1/2}}{x_1^+(x'_3) + x_1^-(x'_3) - 2x_1 - 2\{[x_1^-(x'_3) - x_1][x_1^+(x'_3) - x_1]\}^{1/2}} \right], \quad (24)$$

and

$$K = (x_3'^2 - 1)[x_1^+(x'_3) - x_1][x_1^-(x'_3) - x_1] = (x_1^2 - 1)[x_3^+(x_1) - x_3^-][x_3^-(x_1) - x_3^+]. \quad (25)$$

Equation (24) is given for $+1 < x_3' < L_{y_2^-}.$ The simplest way to see that the branch of the logarithm in Eq. (24) is thus correctly defined is to let $x_2 = x_4$ and $x = y$ [inequalities (10) etc.]; then x_3^- is the upper limit of the physical boundary [Eq. (18)] *regardless of its position on the real axis.* From the rules of Ref. 3 it follows that x_3^- should not under the circumstances give rise to a singularity of B on the physical boundary. It is a simple matter to convince oneself¹⁷ that this can be avoided if and only if x_3^- is not a branch point of $f(x'_3)$ anywhere along the prescribed integration contour for $x_1 > 1,$ which in turn is possible if and only if the logarithm in Eq. (24) is on its principal branch when

$$+1 < x_3' < \min\{L_{y_2^-}, L_{x_4^-}, x_3^\pm\}. \quad (26)$$

Finally all that remains to be shown is that the contour in Eq. (23) should pass *under* the branch points $L_{x_4^+}$ and $L_{y_2^+}$ of $f(x'_3).$ These branch points should not give rise to singularities of B on the physical boundary for $x_3 > 1$ and inequalities (6) and (7) (Ref. 3). Again in order to simplify the discussion we go to the

¹⁴ R. E. Cutkosky, J. Math. Phys. 1, 429 (1960).

¹⁵ The Feynman amplitude for the box graph can be written (see for example Ref. 2) as follows:

$$B \sim \int_0^1 \frac{d\beta_1 d\beta_2 d\beta_3 d\beta_4 d(1 - \sum_{i=1}^4 \beta_i)}{m_1 m_2 \mu_1 \mu_2 [2\beta_1 \beta_2 x_1 + 2\beta_1 \beta_3 x + 2\beta_1 \beta_4 x_4 + 2\beta_2 \beta_3 x_2 + 2\beta_2 \beta_4 y + 2\beta_3 \beta_4 x_3 - \sum_{i=1}^4 \beta_i^2]^2}.$$

Note that each pair $(x, y), (x_1, x_3),$ and (x_2, x_4) appears in the denominator multiplied by a complete set of β_i 's.

¹⁶ See, for example, S. Mandelstam, Phys. Rev. 112, 1344 (1958); C. Fronsdal, R. E. Norton, and K. T. Mahanthappa, J. Math. Phys. 4, 859 (1963); J. Tarski, *ibid.* 1, 149 (1960).

¹⁷ For example let $L_{x_2^-} < x_1 < L_{x_2^+},$ then $L_{x_2^-} < x_3^+ < x_3^- < L_{x_2^+}$ (see Fig. 5). (The contour passes above $L_{x_2^-}$ and $x_3^+.$) If the logarithm in f is not on its principal branch when $1 < x_3' < \min\{L_{x_2^-}, x_3^\pm\},$ then as x_3' approaches x_3^- along the prescribed contour, it will find x_3^- a branch point of $f.$ Hence x_3^- should lie *above* the contour in order to avoid a pinch with the pole at $x_3 + i\epsilon.$ If we now continue $x_1 + i\epsilon$ so that $x_1 > L_{x_2^+},$ x_3^- will loop clockwise (under) $L_{x_2^+}$ dragging the contour along with it ($1 < x_3^- < x_3^+ < L_{x_2^+},$) and thus making a pinch with $x_3 + i\epsilon$ unavoidable.

permutations of the pairs of variables $(x, y), (x_1, x_3),$ and (x_2, x_4) ¹⁵; it is evident that the desired discontinuity is formally identical to the discontinuity across the x -plane normal threshold¹⁶ after relabeling $x \leftrightarrow x_3$ and $y \leftrightarrow x_1.$ [It is also clear that a double dispersion relation in (x_3, x_1) exists and is identical to the usual one in (x, y) up to relabeling.] So we write (up to over-all constant factors)

$$B(x_3) = \frac{1}{\pi} \int_1^\infty \frac{dx'_3}{x'_3 - x_3 - i\epsilon} f(x'_3), \quad (23)$$

where

case $x_2 = x_4, x = y,$ i.e., $L_{x_4^+} = L_{y_2^+} \equiv L_{x_2^+}.$ ⁹ We now let $1 < x_1 < L_{x_2^-};$ then (see Fig. 5) $L_{x_2^+} < x_3^-$ and unless $L_{x_2^+}$ lies *above* the contour it will give rise to a singularity of B on the physical boundary through a pinch with the pole at $x_3 + i\epsilon.$

Our dispersion relation for $B,$ Eq. (23) is now unambiguously determined for the case of inequalities (6)–(9) and hence for any other case by analytic continuation.

III. CONTINUATION TO COMPLEX INTERNAL MASSES

A. Investigation of the Motion of Singularities as Functions of Particle Widths and External Variables

In this section we shall study the motion of the singularities $L_{x_2^\pm}, L_{y_4^\pm}, x_1^\pm$ (x_1 plane), $L_{x_4^\pm}, L_{y_2^\pm}, x_3^\pm$ (x_3' plane) and the corresponding effect on the size of the amplitude squared, $|B|^2,$ as we continue $m_1 \rightarrow m_1 - i\alpha,$ $\alpha > 0,$ $\mu_1 \rightarrow \mu_1 - i\beta,$ $\beta > 0$ and vary the external variables in their physical ranges. The parameters α and β are related to the full width at half-maximum Γ of m_1 and μ_1 by

$$\alpha \equiv \Gamma_m/2, \quad \beta \equiv \Gamma_\mu/2.$$

A convenient model for our investigation, possessing a certain amount of symmetry, is obtained by letting $m_1 = \mu_1 = m,$ ($\alpha = \beta$), and $m_2 = \mu_2 = M_2 = M_4 = \mu$ in Fig. 1(b).

Clearly $x_2 = x_4$ and thus the triangle singularities are at the same points on both the x_1 and $x_3(x_3')$ plane.

Even with $x_2 = x_4$ the problem still retains its full complexity; i.e., the number of singularities and the number of variables has not been essentially reduced.

Because of the large number of cases one would have to examine, and because it would be desirable to get a comparatively simple and clear picture of the essential features, it is advisable to begin by restricting the investigation to the cases for which $x = y.$ We shall assume this to hold throughout the present section,

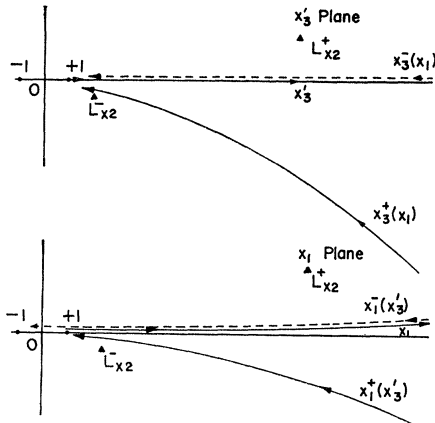


FIG. 6. Motion of the box singularities for $x=y$, $x_2=x_4$ and $s=110$, $\mu=1$, $m=9-i(0.1)$. ($\Gamma \approx 28$ MeV if $\mu=\mu_\pi=1$). $x_3^- = (s-1)^2/2M_1^2 - 1$, so it moves on the real axis.

except where it is otherwise specifically indicated. The $x \neq y$ case will be considered briefly in the following section.

So, we consider the case determined by inequalities (10) (consult last part of Sec. II A with $M=\mu$).

We let $\mu=1$ and $m=9-i(0.1)$, (which would correspond to $\Gamma_m=28$ MeV if $\mu=\text{pion mass}$), and plot the motion of the box singularities x_3^\pm , x_1^\pm as we vary x_1 and x_3 , respectively, keeping $s=t=110$.¹⁸ This is shown in Fig. 6. Note that since x_1 passes under $L_{x_2}^+$, x_3^+ passes over $L_{x_2}^-$ on its way to $+1$ (cf. Fig. 5).

In Figs. 8, 9, and 10 we plot the paths of $L_{x_2}^-$ and x_3^+ as the width parameter α increases from 0 to 0.36 ($\Gamma_m=100$ MeV for $\mu=\text{pion mass}$). The variables s and M_1^2 are fixed in each case so that the singularities lie on the physical boundary when $\alpha=0$.

An examination of the above plots leads to the following conclusions:

(i) x_3^+ is much more sensitive to the variation of the width parameter α than is $L_{x_2}^-$, except when $x_3^+(\alpha=0) \approx L_{x_2}^-(\alpha=0)$, or when α is extremely small; the larger we make $x_3^+(\alpha=0) - L_{x_2}^-(\alpha=0)$, the faster x_3^+ moves downwards with increasing α (Figs. 10 and 8).

(ii) Since x_3^+ on its way to $+1$ passes over $L_{x_2}^-$ as we increase M_1^2 , (keeping x fixed) (see Fig. 6), it is

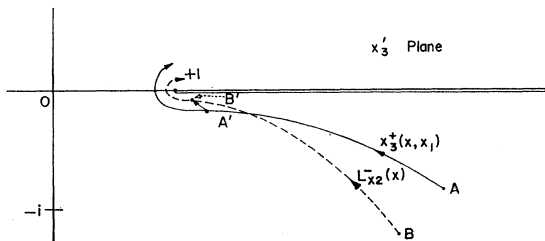


FIG. 7. Relative motion of x_3^- and $L_{x_2}^-$.

¹⁸ Which means that for $\Gamma_m=0$, $x > 1$, $x+x_2 < 0$.

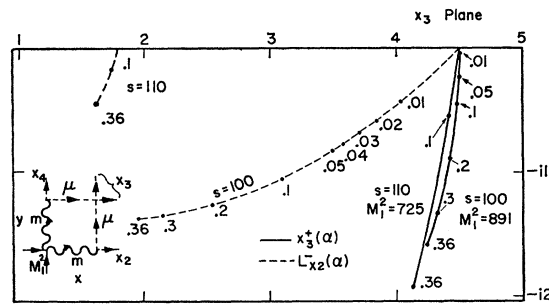


FIG. 8. Motion of the triangle and box singularities. The numbers along the curves denote the value of the width parameter α . For all curves we have $x_2=x_4$, $x=y$, $\mu=1$, $m=9-i(\alpha)$. For purposes of comparison we show two cases, one in which $L_{x_2}^-(\alpha=0) = x_3^+(\alpha=0)$ and the other in which $L_{x_2}^-(\alpha=0) \ll x_3^+(\alpha=0)$.

obvious that we can make $\text{Im}x_3^+ \approx \text{Im}L_{x_2}^-$ for arbitrary α by moving x_3^+ close enough to $L_{x_2}^-$. Now suppose that for some α , $x(s)$, x_2 ¹⁹ and $x_1(M_1^2)$ the singularities are at the points A, B of Fig. 7 with $|\text{Im}x_3^+| < |\text{Im}L_{x_2}^-|$. If we now increase s the singularities will follow the paths of Fig. 7. We see thus that after a certain point $|\text{Im}x_3^+| > |\text{Im}L_{x_2}^-|$. However, if we fix x when x_3^+ and $L_{x_2}^-$ are at the points A', B' , respectively, and increase M_1^2 , x_3^+ will move up to $L_{x_2}^-$ along the path $A'B'$ so that again $|\text{Im}x_3^+| < |\text{Im}L_{x_2}^-|$.

(iii) In general it seems possible that we can always make $|\text{Im}x_3^+| \lesssim |\text{Im}L_{x_2}^-|$ although this most of the time requires *extremely small* α .

(iv) The farther the singularities are from the normal threshold ($+1$) the faster they move downward with increasing α (cf. Figs. 8-10).

So the distance between $L_{x_2}^-$ and x_3^+ when they are on the real x_3 axis ($\alpha=0$) and their distance from $+1$ enables one to guess how they will move as α increases.

B. Amplitude of Box Graph as a Function of Widths and External Variables

For $x_2=x_4$ and $x=y$ the dispersion relation for B [Eqs. (23), (24), and (25)] can be written as follows:

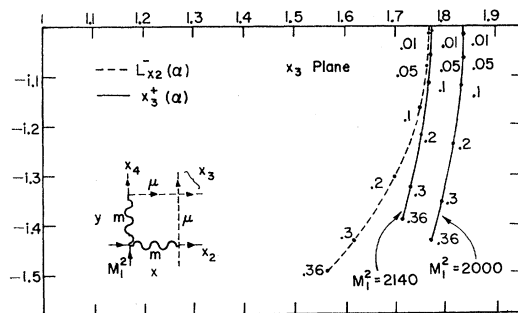


FIG. 9. Motion of the triangle and box singularities. The numbers along the curves denote the value of the width parameter α . For all curves we have $x_2=x_4$, $x=y$, $\mu=1$, $m=9-i(\alpha)$, and $s=110$.

¹⁹ Assuming again $x+x_2 < 0$ for $\alpha=0$.

$$B(x_3) = \frac{1}{\pi} \int_1^\infty \frac{dx_3'}{(x_3' - x_3 - i\epsilon)} \frac{1}{\pi [(x_1^2 - 1)(x_3^+ - x_3')(x_3^- - x_3')]^{1/2}} \times \ln \left[\frac{x_3'(x^2 + x_2^2) + 2xx_2 - x_1(x_3'^2 - 1) + [(x_1^2 - 1)(x_3'^2 - 1)(x_3^+ - x_3')(x_3^- - x_3')]^{1/2}}{x_3'(x^2 + x_2^2) + 2xx_2 - x_1(x_3'^2 - 1) - [(x_1^2 - 1)(x_3'^2 - 1)(x_3^+ - x_3')(x_3^- - x_3')]^{1/2}} \right], \quad (27)$$

where x_3^\pm are now given by Eq. (12).

The integral in Eq. (27) has been evaluated for given x, x_1, x_2, α over a set of x_3 in its physical range [Eq. (18)], using complex-arithmetic FORTRAN IV on the IBM 7094 at the UCLA Computing Facility.

It is worth noting that since the definition of x_3 (or x_3'), Eq. (2), does not involve any of the unstable particle masses, the integration path remains real when $m \rightarrow m - i\alpha$, ($\alpha > 0$), which is convenient in view of our numerical (computer) integration. Furthermore since x_3^- is not a branch point of $f(x_3')$ (see Sec. IIB), in evaluating the integral, one only has to worry about the principal value due to the pole at x_3 (all other singularities being in the complex plane and thus off the integration path).

Since we cannot know *a priori* how close to the physical boundary a singularity (x_3^+ or $L_{x_2}^-$) should be in order to give a reasonably strong peaking, our purpose here has been to investigate, by explicit calculation of the square of the amplitude, $|B|^2$, the effect of x_3^+ (mainly) as we vary α and the external variables.

In general, peaks can be made to appear anywhere within the x_3 physical range by properly adjusting x_1 and x (see for example Fig. 14).

Figure 11 shows in a rather striking way the relative magnitude of the x_3^+ versus the $L_{x_2}^-$ effect (we have used the unrealistic $\alpha = 0.01$ or $\Gamma_m \approx 2.8$ MeV). As expected, the x_3^+ , being an inverse square-root branch point, is much stronger than the logarithmic $L_{x_2}^-$ branch point; hence, when the singularities are close together, the effect one sees is due mainly to x_3^+ . We point out in passing that an interaction proceeding via two ϕ particles ($\Gamma_\phi \approx 3.3 \pm 0.6$) could give rise to such

a striking peak if it were the dominant contribution to the amplitude.

From Fig. 12 we see that, other things being equal, the amplitude enhancement is very sensitive to variation of width; in this example, increasing the width by a factor of 3 (which increases $|\text{Im}x_3^+|$ also by about a factor of 3) cuts down the peak by about a factor of 10. Note, though, that even with as large a width as 84 MeV we still get a fairly well-defined rise in $|B|^2$ near $\text{Re}x_3^+$.

We have plotted in Fig. 13 $|B(x_3)|^2$ for various x_1 and x keeping $\alpha = 0.3$ for all curves; it is interesting that though one might expect the height of the peak to in-

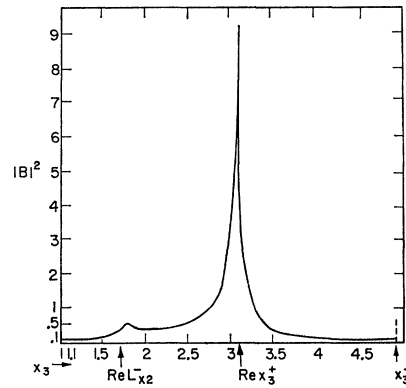


FIG. 11. Triangle and box effects for very small decay width. For this curve we have $x_2 = x_4, x = y, s = 110, M_1^2 = 1000, \alpha = 0.01$ ($\Gamma_m \approx 2.8$ MeV), $L_{x_2}^- \approx 1.77 - i(0.016)$, and $x_3^+ \approx 3.08 - i(0.030)$.

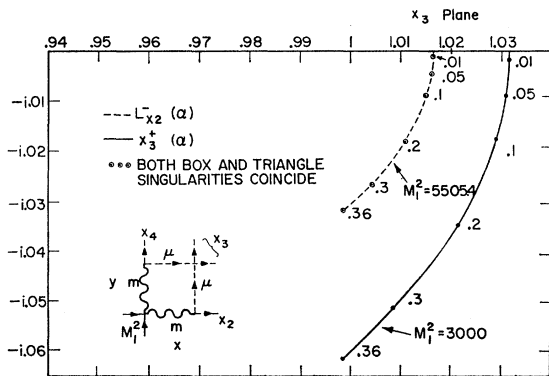


FIG. 10. Motion of the triangle and box singularities. The numbers along the curves denote the value of the width parameter α . For all curves we have $x_2 = x_4, x = y, \mu = 1, m = 9 - i(\alpha)$ and $s = 150$.

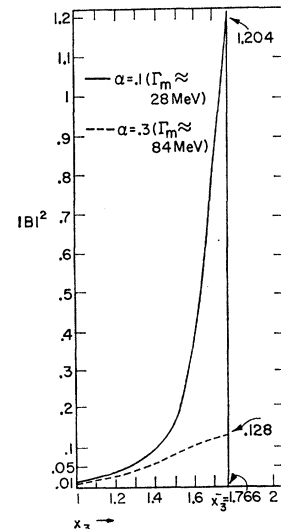


FIG. 12. Effect of decay width variation on $|B|^2$. For both curves $x_2 = x_4, x = y, s = 110, \mu = 1$ (pions), $M_1^2 \approx 2148$. For solid line: $L_{x_2}^- \approx 1.75 - i(0.16), x_3^+ \approx 1.76 - i(0.11)$. For dashed line: $L_{x_2}^- \approx 1.62 - i(0.43), x_3^+ \approx 1.73 - i(0.32)$.

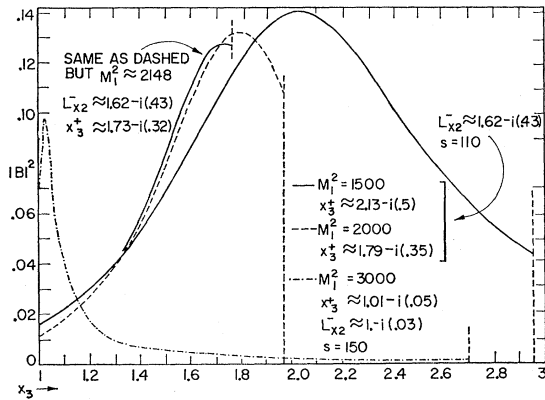


FIG. 13. Variation of $|B|^2$. For all curves $x_2 = x_4$, $x = y$, and $\alpha = 0.3$ ($\Gamma_m \approx 84$ MeV).

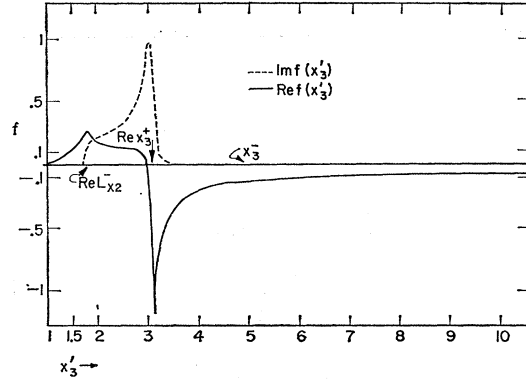


FIG. 15. Variation of the real and imaginary parts of $f(x_3^+)$ for the curve of Fig. 11.

crease as x_3^+ approaches $+1$ and consequently (see Fig. 6) $|\text{Im}x_3^+|$ decrease, what occurs is actually the opposite. This appears to be due to the fact that $f(x_3^+ = 1) = 0$, and thus $\text{Re}f$ and $\text{Im}f$ have narrower peaks than they would if x_3^+ were farther to the right and $\text{Im}x_3^+$ more or less unchanged. It is instructive in this connection to examine in some detail the variation of $\text{Re}f$ and $\text{Im}f$; this variation is shown on Fig. 14 for two of the curves of Fig. 13, and on Fig. 15 for the example of Fig. 11. We stress, however, that because the function we are dealing with is rather complicated, the above inferences should be taken only as rough guides for preliminary orientation to be followed by a more or less detailed investigation of $|B|^2$ for each case of interest.

In the next section we shall continue the investigation of $|B|^2$ as a function of the external variables in connection with two real processes (Γ_m fixed) which have been studied to some extent experimentally.

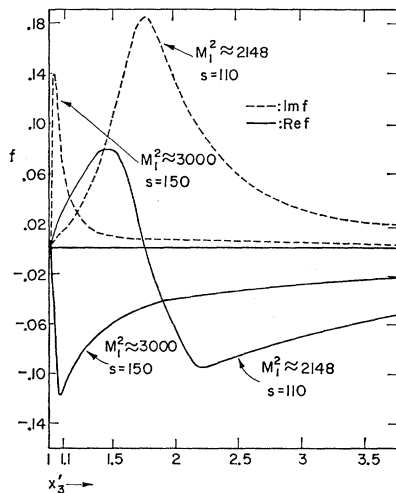


FIG. 14. Variation of the real and imaginary parts of $f(x_3^+)$ for two of the curves of Fig. 13.

IV. APPLICATIONS

A. General Considerations

Let us consider the box graph shown in Fig. 16.²⁰ Here the blobs represent the amplitudes for the processes taking place at the vertices; these amplitudes are unknown functions of the momenta and spin parameters.

As a crude approximation valid only in the neighborhood of the box singularity enhancement we can write

$$A^{(b)} \simeq A^{(r)} A^{(f)} \gamma_1 \gamma_2 \frac{1}{\pi} \int_1^\infty \frac{dx_3'}{x_3' - x_3 - i\epsilon} f = A^{(r)} A^{(f)} \gamma_1 \gamma_2 B(x_3, \dots), \quad (28)$$

where $A^{(r)}$ represents the average effect of the double-resonance production amplitude (Fig. 16) at the incoming center of mass energy (M_1) of interest; similarly $A^{(f)}$ represents the final state interaction for M_3^2 in the neighborhood of the peak, and finally γ_i ($i=1,2$) is proportional to the square root of the decay width of the resonance.

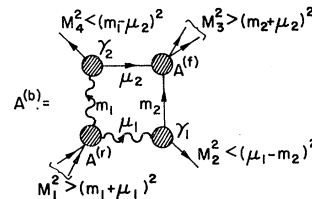


FIG. 16. Exact box graph. $A^{(b)}$ is the exact box amplitude. ($p_i^2 = -M_i^2$.)

²⁰ Readers who have skipped Secs. II and III should consult Eqs. (1) and (2) in conjunction with Fig. 16 so as to familiarize themselves with our notation. We mention here that under our conditions (Table I second case from top) *only* the triangle singularities $L_{y_2}^-, L_{x_2}^-$ and the box singularity x_3^+ can appear on the physical boundary on the x_3 plane (or correspondingly M_3^2 plane). When this happens and $x_3 = L_{y_2}^-, x_3 = L_{x_2}^-,$ or $x_3 = x_3^+$, the graphs shown in Figs. 2(a), 2(b), and 16, respectively, can be thought of as occurring with real intermediate particles (Ref. 3).

We can write the nonresonant final-state²¹ total amplitude A as

$$A = A_0 + A^{(b)}, \quad (29)$$

where A_0 represents all contributions except that of the box graph.

It is impossible to make reliable quantitative estimates of the relative importances of $A^{(b)}$ and A_0 . In fact, a conclusion based upon some attempt to do so might be more misleading than helpful, in as much as an extremely unreliable result may be worse than none. Despite this, however, we use a very crude model and the data in Table II to make a calculation of $A^{(b)}$ relative to A_0 for the reaction discussed in part C of this section, namely, $p\bar{p} \rightarrow \bar{\Lambda}\Lambda\pi^+\pi^-$. It is found that for not unreasonable $\pi^+\pi^-$ scattering lengths, $A^{(b)}$ could compete favorably with, or dominate, A_0 in the neighborhood of the box singularity. What the physical situation is, when the actual angular distributions and phases of all the amplitudes are included, is anybody's guess.

Despite our inability to be quantitative, it is clear that $A^{(b)}$ will have a good chance to dominate over A_0 if $A^{(c)}$ and $A^{(f)}$ in Eq. (28) are "large." It is therefore desirable to look for the box effect in processes where for some M_1^2 there is considerable double-resonance production and at the same time the amplitude $A^{(f)}$ is appreciable. Finally the resonance widths should be neither too large nor too small, since although very small widths would give a high narrow peak in B , the $\gamma_1\gamma_2$ factor would cut down $A^{(b)}$ relative to A_0 , while in the case of very large widths, the situation would be reversed. This behavior has a simple physical interpretation.²² Let us for convenience consider the case where the two resonances involved are the same ($m_1 = \mu_1 = m$). When $x_3 = x_3^+$ and the necessary inequalities hold, the box can be interpreted as a classical process. Introducing widths for the resonances is equivalent to allowing a mass spread around m (i.e., all resonances produced will not have the same mass but their mass spectrum will exhibit the characteristic Breit-Wigner shape).²³ It is clear that $x_3 = x_3^+$ (with all invariants fixed) will be fulfilled only for some events, while for most events particles m_2 and μ_2 will not take off in exactly the right direction for a collision to occur. This has the effect of broadening and decreasing the maximum of the peak centered at x_3^+ , and accounts for the behavior of the peak in B as a function of the width, which is shown in Fig. 12. We note here that taking into account the quantum-mechanical nature of the particles does not essentially alter the above picture.

²¹ Events having one or more resonances in the final state fall in specific Dalitz-plot bands and can be separated out.

²² See C. Kacser, Phys. Letters 12, 269 (1964) and J. B. Bronzan, Phys. Rev. 134, B687 (1964) in connection with triangle graphs.

²³ We recall that in our dispersion relation [see Eq. (28)] the widths appear in B as negative imaginary parts of the masses of the resonances; i.e., for the cases considered here we have $m_1 = \mu_1 = m - i\alpha$, $\alpha = \Gamma/2$ where Γ is the full width at half-maximum.

TABLE II. Relative production rates for processes leading to the final state $\bar{\Lambda}\Lambda\pi^+\pi^-$.

Process	Fraction
(a) $\bar{p}p \rightarrow Y_1^* \bar{Y}_1^*$ (1385)	0.20
(b) $\rightarrow Y_1^* \bar{Y}_1^*$	0.30
(c) $\rightarrow Y_1^* \bar{\Lambda}\pi^-$ and c.c.	0.20
(d) $\rightarrow Y_1^* \bar{\Lambda}\pi^+$ and c.c.	0.10
(e) $\rightarrow \bar{\Lambda}\Lambda\pi^+\pi^-$ (nonresonant)	0.20

On the other hand the resonance width is inversely proportional to the particle lifetime, so that when the width is large the resonances will decay while they are still close to each other and thus particles m_2 and μ_2 will have a chance to interact due to the de Broglie wavelength spreading even if they are not aimed in the right direction. When the width is small, the resonances will get to travel a long distance apart before decaying, and thus even a small deviation from the correct direction will cause m_2 and μ_2 to pass each other a relatively large distance apart. (When the width is zero the "resonances," of course, will never decay.) This behavior is manifested through the over-all γ^2 factor on B [Eq. (28)].

We now turn our attention to two reactions, which we believe might well exhibit the box amplitude enhancement. These are

$$\bar{p}p \rightarrow \bar{\Lambda}\Lambda\pi^+\pi^-, \quad (30)$$

at an incident \bar{p} momentum of 3.7 BeV/c, and

$$\bar{p}p \rightarrow \bar{K}K\pi\pi, \quad (31)$$

at rest.

Proton-antiproton annihilations leading to the final states of reactions (30) and (31) have been studied experimentally²⁴ at the above momenta, and in both cases a rather large amount of double resonance production was found.

We quote in Tables II and III the pertinent data from Ref. 24.

The full width at half-maximum of the Y_1^* (1385)

TABLE III. Proton-antiproton annihilations producing $K^0 K^\pm \pi^\mp \pi^0$.

Process	Rate
(a) $\bar{p}p \rightarrow K^\pm K_1^0 \pi^\mp \pi^0$ (total)	5.19×10^{-3}
(b) $\rightarrow K^{*0} \bar{K}^{*0}$	1.43×10^{-3}
(c) $\rightarrow K^{*+} K^{*-}$	0.77×10^{-3}
(d) $\rightarrow K^{*0} K^0 \pi^\mp$	1.04×10^{-3}
(e) $\rightarrow K^{*0} K^\mp \pi^0$	0.97×10^{-3}
(f) $\rightarrow K^{*0} K^\pm \pi^\mp$	0.57×10^{-3}

* For the various rates in the annihilations leading to the final states $K_1 K_1 \pi^+ \pi^-$ and $K_1 (K^0) \pi^+ \pi^-$, see Ref. 24.

²⁴ For annihilations into $\bar{\Lambda}\Lambda\pi^+\pi^-$ see C. Baltay, J. Sandweiss, H. D. Taft, B. B. Culwick, J. K. Kopp, R. J. Louttit, R. P. Shutt, and A. M. Thorndike, Phys. Rev. 140, B1027 (1965); for annihilations into $\bar{K}K\pi\pi$ see N. Barash, L. Kirsch, D. Miller, and T. H. Tan, *ibid.* 145, 1095 (1966) and references therein. We are indebted to the authors for sending us their results prior to publication.

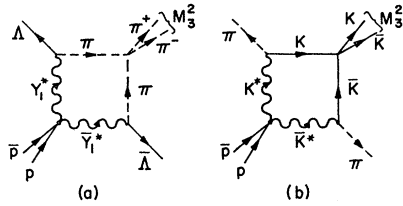


FIG. 17. Box graphs contributing to the nonresonant final state in reactions (30) and (31).

resonance is 53 MeV while that of the K^* is 50 MeV,²⁵ so we have in units of the pion mass

$$\frac{1}{2}\Gamma_{Y^*} = \alpha_{Y^*} = 0.19 \quad \text{and} \quad \frac{1}{2}\Gamma_{K^*} = \alpha_{K^*} = 0.179.$$

The box graphs that we study in connection with reactions (30) and (31) are shown in Fig. 17.

Anticipating the results of the following sections [in both cases the peaks appear close to the M_3^2 threshold ($x_3 \simeq 1$)], we would want the $\pi^+\pi^-$ and $\bar{K}K$ scattering amplitudes and in particular the S -wave scattering lengths to be large.

The S -wave $\pi^+\pi^-$ elastic scattering amplitude $A_{\pi^+\pi^-}$ is given in terms of the (S -wave) isotopic spin amplitudes A_T by

$$A_{\pi^+\pi^-} = \frac{1}{3}(A_2 + 2A_0). \quad (32)$$

Experimental evidence points to a strong S -wave $T=0$, $\pi\pi$ scattering length effect.²⁶ A reasonable set of values for the scattering lengths appears to be²⁷

$$a_0 \simeq 1\lambda_\pi, \\ a_2 \simeq 0.12\lambda_\pi.$$

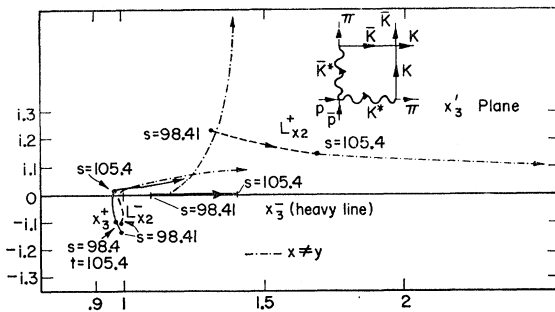


FIG. 18. Motion of singularities for $p\bar{p} \rightarrow K\bar{K}\pi\pi$ [annihilation at rest, $M_1^2 = 180.8$, $\mu_\pi = 1$, $m_{K^*} = 6.38 - i(0.179)$]. In the $x \neq y$ parts $L_{x_2^-}$ ($s = 98.41$) is fixed, while $L_{y_2^-}(t)$ and the rest move as t increases from 98.41 to 154.8. ($t \leq (M_1 - M_4)^2 \simeq 155.0$.)

²⁵ A. H. Rosenfeld *et al.*, University of California Radiation Laboratory Report No. UCRL-8030, 1964 (unpublished). The later values for these widths appeared during the course of this calculation [A. H. Rosenfeld *et al.*, *Rev. Mod. Phys.* **37**, 633 (1965)] and are $\Gamma_{Y_1^*(1385)} = 44$ MeV, $\Gamma_{K^*} = 49$ MeV; they would improve our peaks slightly.

²⁶ N. E. Booth and A. Abashian, *Phys. Rev.* **132**, 2314 (1964); J. Kirz, J. Schwartz, and R. D. Tripp, *ibid.* **130**, 2481 (1963); T. Maung, K. M. Crowe, and N. T. Dairiki, *Phys. Rev. Letters* **16**, 374 (1966). P. D. B. Collins, *Phys. Rev.* **142**, 1156 (1966); see however, F. T. Meiere and M. Sugawara, *ibid.* **153**, 1702 (1967).

²⁷ J. Kirz, J. Schwartz, and R. D. Tripp, *Phys. Rev.* **126**, 763 (1962); Aachen-Birmingham-Bonn-Hamburg-London (I.C.)-München Collaboration, *Nuovo Cimento* **31**, 485 (1964).

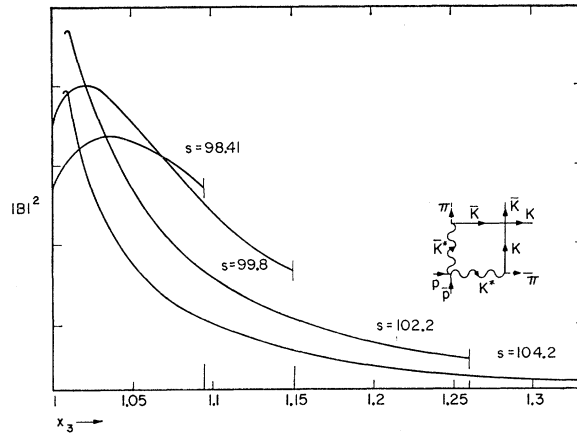


FIG. 19. Variation of $|B|^2$ for the case $p\bar{p} \rightarrow K\bar{K}\pi\pi$.

Unfortunately, there is no experimental information on $\bar{K}K$ scattering, but we would expect $A^{(\prime)}$ for the box graph of Fig. 17(b) to be roughly as large as the $\pi^+\pi^-$ amplitude. [For example, $SU(3)$ and octet dominance give $\langle \pi^+\pi^- | \pi^+\pi^- \rangle / \langle K^+K^- | K^+K^- \rangle = 1$.]

B. $p\bar{p} \rightarrow \bar{K}K\pi\pi$

In this section we study the possibility of an enhancement arising from the graph of Fig. 17(b). Clearly we have $x_2 = x_4$, and we proceed by setting $s = t$ or equivalently $x = y$ without loss of generality since we would have to look for the peaks in x_3 for some fixed x and y anyway; we shall, however, consider later the effect of making $x \neq y$.

All masses, etc., in this and the next section are measured in pion mass units. Thus for proton-antiproton annihilation at rest we have $M_1^2 \simeq 180.8$, $m_{K^*} \simeq 6.38 - i(0.179)$,²⁸ while

$$+1 \leq x \leq -x_2 \quad \text{or equivalently} \quad 98.41 \leq s \leq 105.4; \quad (33)$$

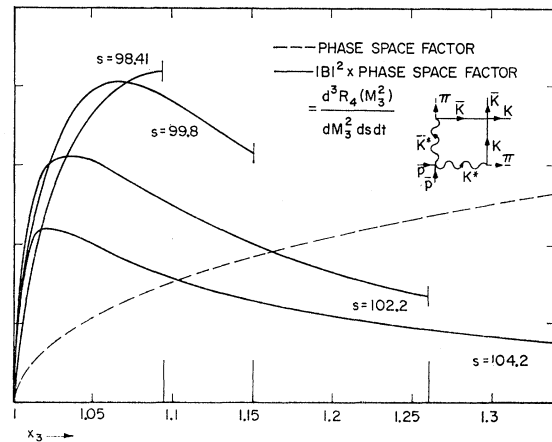


FIG. 20. Effect of phase-space factor on the curves of Fig. 19.

i.e., for s larger than the upper limit, the triangle singularity will loop clockwise around $x_3 = +1$ and move onto the upper half plane of the second Riemann sheet of the amplitude B . (Cf. Fig. 3.)

Figure 18 shows the paths of $L_{x_2}^{\pm}$ ⁹ (dashed lines) and x_3^{\pm} (solid lines)²⁸ on the x_3' plane. We remark that although x_3^+ has gone through the $L_{x_2}^-$ cut (which we take parallel to the real axis from $L_{x_2}^-$ to $+\infty + i \text{Im} L_{x_2}^-$), both singularities stay rather close to the real axis. [Recall that the physical range of x_3 extends from $+1$ to x_3^- , see Eq. (18)]. In Fig. 19 we have plotted some typical $|B|^2$ curves (arbitrary units) for s varying through practically the entire (33) range. The best peak is that for $s \simeq 102.2$; however, we have more-or-less good peaks throughout the entire range getting narrower as s approaches 105.

We now calculate the three-dimensional partial distribution of events for fixed M_1^2 , s , and t as a consequence of the matrix element squared $|B|^2$. This is

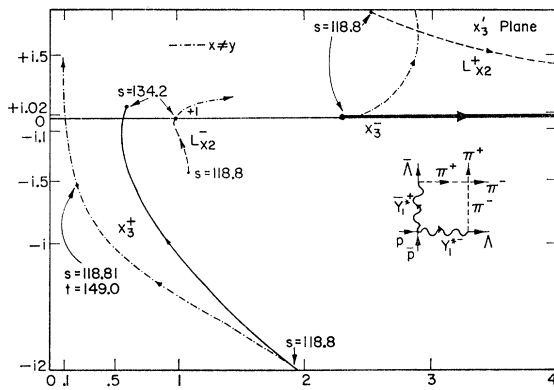


FIG. 21. Motion of singularities for $p\bar{p} \rightarrow \Lambda\bar{\Lambda}\pi^+\pi^-$ [annihilation at 3.7 BeV/c, $M_1^2=456.9$, $\mu_\pi=1$, $m_{Y^*}=9.9-i(0.19)$]. In the $x \neq y$ parts $L_{x_2}^-$ ($s=118.8$) is fixed, while $L_{y_2}^-$ (t) and the rest move as t increases from 118.81 to 179.0. [$t \leq (M_1 - M_4)^2 \simeq 179.3$]

given by²⁹

$$\frac{d^3 R_4}{ds dt dM_3^2} \sim \frac{\pi^3}{8M_1^2} \left(\frac{x_3 - 1}{x_3 + 1} \right)^{1/2} |B|^2, \quad (34)$$

with the boundaries given by Eqs. (15) through (18). In Fig. 20 we compare the density of events given by Eq. (34) (solid lines) for the $|B|^2$ shown in Fig. 19, with that of pure phase space (dashed lines). Since the scale for $|B|^2$ is arbitrary, it is the shape of the curves that is significant. We conclude that for $s \simeq t \simeq 102$, one should be able to detect a comparatively large accumulation of events near threshold. Returning to Fig. 18 we let $s=98.4$, i.e., $L_{x_2}^-$ is at the lower end of its path, and increase t ; thus $L_{y_2}^-$ follows the (dashed) path that $L_{x_2}^-$ followed before (when $s=t$). It turns out that x_3^+

²⁸ Dash-dot curves refer to the $x \neq y$ case and should be ignored at this point.

²⁹ See, for example, P. Nyborg, H. S. Song, W. Kernan, and R. H. Good, Jr., Phys. Rev. 140, B914 (1965).

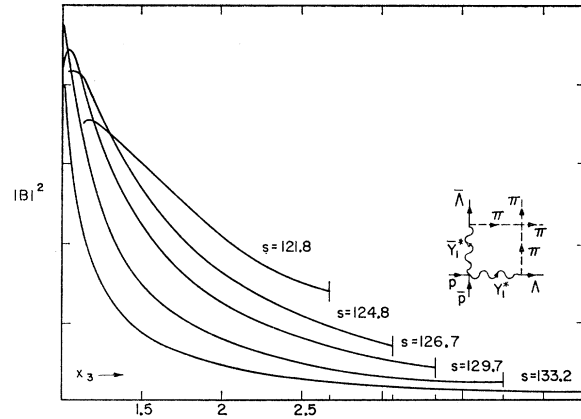


FIG. 22. Variation of $|B|^2$ for the case $p\bar{p} \rightarrow \Lambda\bar{\Lambda}\pi^+\pi^-$.

follows the same path as before.³⁰ We indicate the position of x_3^+ when $L_{x_2}^-$ is at the lower end and $L_{y_2}^-$ is about to loop around $+1$. We therefore expect little change in the curves of Fig. 20 for $s \neq t$ (but not too different). (It is in fact conceivable, since x_3^+ remains close to the physical boundary for a great part of the s and t ranges, that if the box graph dominates sufficiently over the background, the enhancement may survive in the integrated distribution dR_4/dM_3^2 .)

C. $\bar{p}p \rightarrow \bar{\Lambda}\Lambda\pi^+\pi^-$

For the graph of Fig. 17(a) we again have $x_2=x_4$, and as in the previous case we set $s=t$ ($x=y$). Here $M_1^2 \simeq 456.9$, $m_{Y^*} \simeq 9.9 - i(0.19)$,²³ while

$$+1 \leq x \leq -x_2 \quad \text{or equivalently} \quad 118.81 \leq s \leq 134.18. \quad (35)$$

Figure 21 shows the paths of $L_{x_2}^{\pm}$ (dashed lines) and x_3^{\pm} (solid lines)²⁸ on the x_3' plane. The singularities $L_{x_2}^-$ and x_3^+ are farther away from the physical boundary than in the previous case. We do, however, get good peaks for $122 \leq s \leq 133$ (see Fig. 22), the best one being that for $s \simeq 129.7$.

In Fig. 23 we compare the corresponding partial distributions of events [see Eq. (34)] with that for pure phase space. Again we conclude that one can reasonably expect a relatively large accumulation of events near threshold for $s \simeq t \simeq 129.7$.

Finally we examine briefly the motion of the singularities for $s \neq t$ ($x \neq y$). Setting $s=118.81$, we increase t . The singularity $L_{y_2}^-$ follows the path previously followed by $L_{x_2}^-$ and subsequently moves on the upper half-plane of the second Riemann sheet, while x_3^{\pm} follow the paths shown in Fig. 21 (dash-dot lines). We note that under the circumstances the path of x_3^+ is farther from the physical boundary than before and therefore we should expect the peaks to flatten out as

³⁰ x_3^- is now complex (dash-dot line) so that the physical x_3 range is given by (16) and (17).

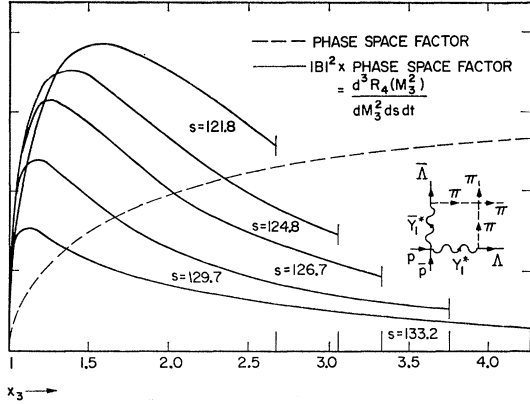


FIG. 23. Effect of the phase-space factor on the curves of Fig. 22.

s becomes different from t . Thus it is clear that the $s=t$ cases are the best cases for experimental study.

ACKNOWLEDGMENTS

One of us (P. C.) wishes to thank Professor E. S. Abers, Professor R. C. Arnold, Professor L. A. P. Balázs, Professor M. Parkinson, and W. M. Dunwoodie for helpful discussions. We wish to thank Eugene Colton for his computer evaluation of a phase-space factor. A computer-time grant by the UCLA Computing Facility is gratefully acknowledged.

APPENDIX

We obtain here a crude estimate of the ratio $|A^{(b)}|^2/|A|^2$ for the $\bar{p}p \rightarrow \bar{\Lambda}\Lambda\pi^+\pi^-$ case, which we treat in Sec. IVC. The amplitudes $A^{(b)}$ and A are defined at the beginning of Sec. IV.

We use a field-theoretic model in which all fields are scalar and carry charge (or strangeness). The effective interaction Hamiltonian density is given by

$$\begin{aligned} \mathcal{H}_I = & \gamma_{Yp} : \phi_Y^* \phi_Y \phi_p^* \phi_p : \\ & + \gamma_{Y\Lambda\pi} : (\phi_Y^* \phi_\Lambda \phi_\pi + \phi_Y \phi_\Lambda^* \phi_\pi^*) : \\ & + \gamma_{\pi\pi} : \phi_\pi^* \phi_\pi \phi_\pi^* \phi_\pi : . \end{aligned} \quad (\text{A1})$$

Using this Hamiltonian, we find for the box amplitude $A^{(b)}$

$$A^{(b)} = \frac{\gamma_{Yp} \gamma_{Y\Lambda\pi}^2 \gamma_{\pi\pi}}{16m_Y^2 m_\pi^2} B, \quad (\text{A2})$$

where B is defined by Eqs. (23) and (24). [An over-all factor of $\frac{1}{2}$ missing from Eq. (24) has been incorporated in the factor that multiplies B in Eq. (A2).] Similarly, we find

$$\Gamma_Y = \frac{\gamma_{Y\Lambda\pi}^2}{4\pi m_Y^2} \left(\frac{1}{2} \right) \left[\frac{\Delta(m_Y^2, m_\Lambda^2, m_\pi^2)}{4m_Y^2} \right]^{-1/2}, \quad (\text{A3})$$

where Γ_Y is the $Y_1^*(1385)$ width (see Sec. IVA). The effective coupling constants γ_{Yp} and $\gamma_{\pi\pi}$ appearing in Eq. (A2) are connected to the total cross sections for $\bar{p}p \rightarrow \bar{Y}^* Y^*$ and $\pi^+\pi^- \rightarrow \pi^+\pi^-$, respectively, by

$$\sigma_{YY} = \frac{\gamma_{Yp}^2}{(2\pi)^2 2\omega_{\bar{p}} 2\omega_p |v_{\bar{p}} - v_p|} W_2, \quad (\text{A4})$$

and

$$\sigma_{\pi\pi} = \gamma_{\pi\pi}^2 / \pi M_3^2, \quad (\text{A5})$$

where W_n is the n -particle invariant phase space and M_3 the two-pion c.m. energy.

Finally, using the effective interaction Hamiltonian density

$$\mathcal{H}_I = \gamma : \phi_\Lambda^* \phi_\Lambda \phi_\pi^* \phi_\pi \phi_p^* \phi_p :$$

we get

$$A = \gamma, \quad (\text{A6})$$

and for the total nonresonant final-state cross section

$$\sigma_{\Lambda\Lambda\pi\pi} = \frac{\gamma^2}{(2\pi)^8 2\omega_{\bar{p}} 2\omega_p |v_{\bar{p}} - v_p|} W_4. \quad (\text{A7})$$

Now, from the experimental results appearing in Table II [reactions (a), (b), and (e)] we have that

$$\sigma_{YY} / \sigma_{\Lambda\Lambda\pi\pi} = 5/2. \quad (\text{A8})$$

Equation (A8) along with (A4), (A6), and (A7) gives the ratio

$$\frac{\gamma_{Yp}^2}{|A|^2} = \frac{1}{(2\pi)^6} \left(\frac{5}{2} \right) \frac{W_4}{W_2}, \quad (\text{A9})$$

so that using Eqs. (A9), (A2), (A3), and (A5), we obtain

$$\frac{|A^{(b)}|^2}{|A|^2} = \frac{\Gamma_Y^2 m_Y^2 \sigma_{\pi\pi} (x_3 + 1) |B|^2 5W_4}{\Delta(m_Y^2, m_\Lambda^2, m_\pi^2) 8m_\pi^2 (2\pi)^3 W_2}, \quad (\text{A10})$$

where

$$x_3 + 1 = M_3^2 / 2m_\pi^2.$$

For the cases shown in Fig. 22, we find that in the range $1.02 \leq x_3 \leq 1.57$ or equivalently $280.6 \text{ MeV} \leq M_3 \leq 316.5 \text{ MeV}$, we have on the average $(x_3 + 1) |B|^2 \approx 8.6$. Thus, for example, in order to have $|A^{(b)}|^2 / |A|^2 \approx 1$, we need $\sigma_{\pi\pi} \approx 160 \text{ mb}$ near threshold; this cross section corresponds roughly to an S -wave, $I=0$, $\pi\pi$ scattering length $|a_0| \approx 1.2$ pion Compton wavelengths. A scattering length of this magnitude is not unreasonable²⁶ (see in particular Collins who reviews the situation). We remark also that since $A = A_0 + A^{(b)}$ we could in general have box dominance over A_0 even if $|A^{(b)}|^2 / |A|^2 < 1$.